

Stochastic TDHF in an exactly solvable model

L. Lacombe

Laboratoire de Physique Théorique, Université de Toulouse, CNRS, UPS, France

E. Suraud

Laboratoire de Physique Théorique, Université de Toulouse, CNRS, UPS, France

P.-G. Reinhard

*Institut für Theoretische Physik, Universität Erlangen, Staudtstraße 7, D-91058
Erlangen, Germany*

P. M. Dinh¹

Laboratoire de Physique Théorique, Université de Toulouse, CNRS, UPS, France

Abstract

We apply in a schematic model a theory beyond mean-field, namely Stochastic Time-Dependent Hartree-Fock (STDHF), which includes dynamical electron-electron collisions on top of an incoherent ensemble of mean-field states by occasional 2-particle-2-hole ($2p2h$) jumps. The model considered here is inspired by a Lipkin-Meshkov-Glick model of Ω particles distributed into two bands of energy and coupled by a two-body interaction. Such a model can be exactly solved (numerically though) for small Ω . It therefore allows a direct comparison of STDHF and the exact propagation. The systematic impact of the model parameters as the density of states, the excitation energy and the bandwidth is presented and discussed. The time evolution of the STDHF compares fairly well with the exact entropy, as soon as the excitation energy is sufficiently large to allow $2p2h$ transitions. Limitations concerning low energy excitations and memory effects are also discussed.

Keywords: TDDFT, dissipation, stochastic jumps

¹corresponding author : dinh@irsamc.ups-tlse.fr

1. Introduction

Time-dependent mean-field methods are widely used tools to describe the dynamics of many-fermion systems, for example in the framework of time-dependent density functional theory in electronic systems [1, 2, 3] or of time-dependent Hartree-Fock (TDHF) in nuclei [4, 5, 6]. However, at high excitations and/or over long simulation times, dynamical correlations, neglected in mean-field propagation, become increasingly important. These have been studied extensively in homogeneous systems as quantum liquids [7, 8]. Dynamical correlations for finite systems are much more demanding and have been treated mostly in semi-classical approximation by the Vlasov-Uehling-Uhlenbeck (VUU) approach which has found wide spread application, e.g., in nuclear physics [9, 10], in laser excitation of metal clusters [11, 12, 3], or in electron transport in wires [13]. A fully quantum-mechanical description of dynamical correlations in finite fermion systems is much more demanding. One promising line of development is Stochastic TDHF (STDHF) where correlations are handled in terms of an ensemble of mean-field states generated by stochastic jumps into 2-particle-2-hole states [14, 15]. Recently, first practical tests came up in one-dimensional many-electron systems [16, 17].

The aim of this paper is to continue testing of STDHF by comparison with an exact solution. To this end, we employ a sufficiently simple schematic model. Starting point is the Lipkin-Meshkov-Glick (LMG) model [18, 19, 20]. It reduces the dynamics in many-body systems to one degenerated band of occupied levels and another degenerated band of unoccupied levels modeling the typical energy separation of the HOMO-LUMO gap in closed shell systems. A two-body interaction is added which generates one prominent coherent resonance excitation. Depending on the interaction strength, one can simulate a variety of many-body effects as, e.g., spontaneous symmetry breaking or large-amplitude collective motion and it has been used for this purpose particularly in nuclear physics [21]. The LMG model is closely related to models of coupled spin-1/2 systems as used in quantum optics [22]. The difference lies mainly in the shaping of interaction which ranges all over the system in the LMG model while nearest neighbor coupling is often used in other realizations. The LMG model has also been used as a test model in a nuclear context [23, 24, 25, 26]. It can be modified to allow for a description of dissipation by allowing a certain spread of excitation energies over the levels [27]. The energies of the levels are distributed stochastically and that is why we called this extension a Stochastic Two-Level Model (STLM).

The simplicity of the model allows an exact solution and so we use STLM here for testing STDHF.

The paper is organized as follows. In Sec. 2, we first present the the STLM, then the TDHF, the STDHF and the exact propagation thereof. We also detail the initial excitation used and the observables studied in this work. And we finally end the theory section on numerical technicalities. In Sec. 3, we discuss the corresponding results : we start with a typical test case and then study the impact of varying the model parameters and the initial excitation. We finally give some conclusions and perspectives in Sec. 4.

2. Theoretical framework

2.1. A stochastic two-level model

The STLM is sketched in Fig. 1. The model consists in two bands of

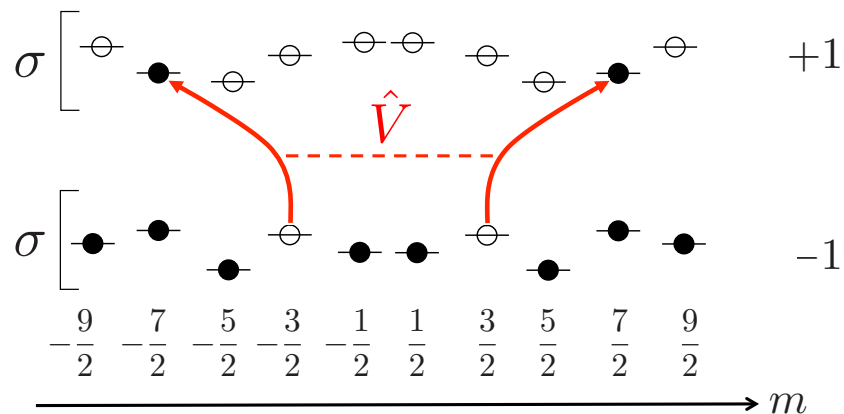


Figure 1: Illustration of the Stochastic Two-Level Model with the action of \hat{V} , defined in Eq. (2c), applied to the ground state of \hat{H}_0 , defined in Eq. (2b), for $j = 9/2$.

single-particle (s.p.) levels, the lower band denoted by the principle quantum number $s = -1$ and the upper one by $s = +1$. Each band contains an even number of Ω levels denoted by the secondary quantum number m running from $-j$ to $+j$ in steps of 1 such that $\Omega = 2j + 1$ (and j is then half integer). In the example displayed in Fig. 1, the $j = 9/2$ yields a sub-shell with 10 different m values from $-9/2$ to $+9/2$. S.p. states are thus represented by a combined quantum number :

$$\alpha = (s_\alpha, m_\alpha) , s_\alpha \in \{-1, +1\} , m_\alpha \in \{-j, -j+1, \dots, j-1, j\} . \quad (1a)$$

The states are grouped into $\pm m_\alpha$ partners and we keep this symmetry to reduce the complexity. For compact notation, we introduce the following abbreviations wherever convenient

$$\bar{m}_\alpha = -m_\alpha, \quad \bar{\alpha} = (s_\alpha, \bar{m}_\alpha) = (s_\alpha, -m_\alpha) \equiv -\alpha. \quad (1b)$$

The notion $\alpha > 0$ then means $m_\alpha > 0$.

The model Hamiltonian consists out of one-body Hamiltonian \hat{H}_0 plus two-body interaction \hat{V} . It is constructed in a standard manner on the basis of annihilation (and creation) operators $\hat{a}_{s_\alpha, m_\alpha}^{(\dagger)} = \hat{a}_\alpha^{(\dagger)}$ for each s. p. state as :

$$\hat{H} = \hat{H}_0 + \hat{V}, \quad (2a)$$

$$\hat{H}_0 = \sum_\alpha \frac{s_\alpha \varepsilon_\alpha}{2} \hat{a}_\alpha^\dagger \hat{a}_\alpha, \quad (2b)$$

$$\hat{V} = v_0 \hat{S}_+ \hat{S}_-, \quad (2c)$$

$$\hat{S}_+ = \sum_{\alpha > 0} \hat{a}_\alpha^\dagger \hat{a}_{\bar{\alpha}}^\dagger = (\hat{S}_-)^\dagger, \quad (2d)$$

$$\varepsilon_\alpha = \Delta + \delta\varepsilon_\alpha, \quad (2e)$$

$$\delta\varepsilon_\alpha : \sum_{m_\alpha} \delta\varepsilon_\alpha \xrightarrow{\Omega \rightarrow +\infty} 0, \quad \frac{1}{\Omega} \sum_{m_\alpha} (\delta\varepsilon_\alpha)^2 \xrightarrow{\Omega \rightarrow +\infty} \sigma^2, \quad (2f)$$

where Δ stands for the average level spacing between the two shells $s = -1$ and $s = +1$ and the $\delta\varepsilon_\alpha$ are chosen stochastically according to a Gaussian distribution with width σ and centroid zero. The gap Δ defines the energy unit and the time unit is accordingly $[\Delta^{-1}]$. We shall use these units all over the text. With $\sigma = 0$, the model reduces to the case with fully degenerated bands. Finally, v_0 describes the strength of the coupling \hat{V} . This interaction is in the form of a pairing interaction as used in the seniority model or BCS (see sections 6.2 and 6.3 of [28]). It models in most simple manner collisions between α - $\bar{\alpha}$ pairs of fermions.

In the following, we always consider half-filled systems such that the particle number becomes $N = \Omega$. In addition, we only consider weak and repulsive interactions $v_0 > 0$. This minimizes the effect of \hat{V} on the ground state such that \hat{V} serves mainly to induce correlations. From a more physical perspective, it also mocks up typical systems in which the mean-field provides a good description of ground state properties. This is also well suited for our purpose to study the treatment of dynamical correlations with STDHF. The

ground state $|\Phi_0\rangle$ of the free Hamiltonian \hat{H}_0 possesses all electrons in the lower band $s = -1$. This feature is still approximately correct for the weak interactions \hat{V} considered here and it remains even exact at Hartree-Fock (HF) level.

2.2. The Hartree-Fock (HF) approach

The operator \hat{a}_α^\dagger creates a single particle (s.p.) basis state and \hat{a}_α annihilates it. The creation operator for any other s.p. state is obtained by the linear combination

$$\hat{b}_\kappa^\dagger = \sum_{\alpha>0} \hat{a}_\alpha^\dagger A_{\alpha\kappa} \quad , \quad \hat{b}_{\bar{\kappa}}^\dagger = \sum_{\alpha>0} \hat{a}_{\bar{\alpha}}^\dagger A_{\bar{\alpha}\bar{\kappa}} \quad , \quad (3)$$

where $\kappa > 0$ and $\bar{\kappa} = -\kappa$. The symmetry of \hat{H} allows us to skip the cross couplings $\alpha \leftrightarrow \bar{\kappa}$ and $\bar{\alpha} \leftrightarrow \kappa$. A general independent-particle state (Slater state) for $N = \Omega$ particles is generated by applying all \hat{b}_κ^\dagger :

$$|\Phi\rangle = \hat{b}_{\kappa_1}^\dagger \hat{b}_{\kappa_2}^\dagger \dots \hat{b}_{\kappa_\Omega}^\dagger |\text{vac}\rangle \quad . \quad (4)$$

The energy expectation value of this state is the Hartree-Fock energy

$$\begin{aligned} E_{\text{HF}} &= \langle \Phi | \hat{H} | \Phi \rangle \\ &= \frac{1}{2} \sum_{m_\alpha > 0} \varepsilon_{m_\alpha} (\rho_{1m_\alpha, 1m_\alpha} - \rho_{-1m_\alpha, -1m_\alpha}) + v_0 \sum_{\alpha, \alpha' > 0} \rho_{\alpha'\alpha} \rho_{\bar{\alpha}'\bar{\alpha}} \quad , \quad (5a) \end{aligned}$$

$$\rho_{\alpha'\alpha} = \langle \Phi | \hat{a}_\alpha^\dagger \hat{a}_{\alpha'} | \Phi \rangle = \sum_{\kappa > 0} n_\kappa A_{\alpha\kappa}^* A_{\alpha'\kappa} \quad , \quad (5b)$$

$$\rho_{\bar{\alpha}'\bar{\alpha}} = \langle \Phi | \hat{a}_{\bar{\alpha}}^\dagger \hat{a}_{\bar{\alpha}'} | \Phi \rangle = \sum_{\kappa > 0} n_\kappa A_{\bar{\alpha}\bar{\kappa}}^* A_{\bar{\alpha}'\bar{\kappa}} \quad , \quad (5c)$$

where $\rho_{\alpha'\alpha}$ is the one-body density matrix and n_κ is the occupation number of state κ . The ground state of the mean-field approximation is obtained by minimizing E_{HF} with respect to the $\rho_{\alpha'\alpha}$ or to $A_{\alpha'\kappa}$. For the regime of weak $v_0 > 0$ which we are studying, the mean-field ground state $|\Phi_0\rangle$ of the interacting system is identical to the ground state of \hat{H}_0 which is given by the trivial non-transformation $A_{\alpha\kappa} = \delta_{\alpha\kappa}$.

The TDHF equations are derived by the time-dependent variational principle [29] and solved in practice by expressing them in terms of the amplitudes $A_{\alpha\kappa}(t)$, yielding

$$i\hbar \partial_t A_{\alpha\kappa} = \sum_{\alpha'} \hat{h}_{\alpha\alpha'} A_{\alpha'\kappa} \quad , \quad \hat{h}_{\alpha\alpha'} = \frac{\varepsilon_{m_\alpha}}{2} s_\alpha \delta_{\alpha\alpha'} + \rho_{\bar{\alpha}'\bar{\alpha}} \quad . \quad (6)$$

The numerical solution is done using an implementation of the Crank-Nicolson scheme [30]

$$\hat{A}(t+dt) = \frac{1 - \frac{idt}{2\hbar}\hat{h}(t + dt/2)}{1 + \frac{idt}{2\hbar}\hat{h}(t + dt/2)}\hat{A}(t) \quad , \quad (7)$$

where \hat{A} is a compact notation of the matrix $A_{\alpha\kappa}$ of expansion coefficients. $\hat{h}(t+dt/2)$ is computed in a predictor step which looks like the full step (7) but propagating only by $dt/2$ and using $\hat{h}(t)$. The Crank-Nicolson step maintains ortho-normality by construction. To obtain satisfying energy conservation, one has to choose the step size dt sufficiently small.

2.3. Stochastic Time-Dependent Hartree Fock (STDHF)

Mean-field propagation with TDHF, as outlined in Sec. 2.2, takes only part of the two-body interaction \hat{V} into account. There remains a residual interaction from \hat{V} which generates correlations. The idea in STDHF is to simplify the description of those correlations by expressing a correlated state as an (incoherent) ensemble of mean-field states and the propagation of correlations by occasional two-particle-two-hole ($2p2h$) jumps [14, 16], which makes sense in dynamical regimes attained at sufficiently high excitation energies, when exploring dense enough excitation spectra. The idea is somewhat similar to the ideas underlying the derivation of the semi-classical Vlasov-Uehling-Uhlenbeck (VUU) approach [9, 31], where dynamical correlations are reduced to incoherent two-particle collisions. It can even be formally shown that STDHF, once properly averaged, reduces to the stochastic Boltzmann-Langevin equation [14].

The state of the system is described by an ensemble of Slater states

$$\{|\Phi^{(i)}(t)\rangle, i = 1, \dots, \mathcal{N}_{\text{ens}}\} \quad . \quad (8)$$

Although not computed explicitly, we assume that each state is allowed to develop $2p2h$ correlations as :

$$|\Phi^{(i)}\rangle \longrightarrow |\Psi^{(i)}\rangle = c_0^{(i)}|\Phi^{(i)}\rangle + \sum_{\kappa_1\kappa_2\kappa_3\kappa_4} c_{\kappa_1\kappa_2\kappa_3\kappa_4}^{(i)}|\Phi_{\kappa_1\kappa_2\kappa_3\kappa_4}^{(i)}\rangle, \quad (9a)$$

$$|\Phi_{\kappa_1\kappa_2\kappa_3\kappa_4}^{(i)}\rangle = (\hat{b}_{\kappa_1}^{(i)})^\dagger (\hat{b}_{\kappa_2}^{(i)})^\dagger \hat{b}_{\kappa_3}^{(i)} \hat{b}_{\kappa_4}^{(i)}|\Phi^{(i)}\rangle, \quad (9b)$$

where κ_1, κ_2 are unoccupied states and κ_3, κ_4 occupied ones. For simplicity, we did not write explicitly the time argument in the wave functions and operators. After a certain time of propagation τ_{sample} , the coherent state

(9b) is decomposed into an incoherent ensemble of mean-field states, which are attainable in a probabilistic manner after this incoherent reduction. We can then evaluate transition probabilities in time-dependent perturbation theory. This yields the transition probabilities for a jump from the Slater state $|\Phi^{(i)}\rangle$ to the Slater state $|\Phi_{\kappa_1\kappa_2\kappa_3\kappa_4}^{(i)}\rangle$ as

$$w_{\kappa_1\kappa_2\kappa_3\kappa_4} = \mathcal{P}_{\kappa_1\kappa_2\kappa_3\kappa_4} \tau_{\text{sample}} \quad (10a)$$

$$\mathcal{P}_{\kappa_1\kappa_2\kappa_3\kappa_4} = \frac{2\pi}{\hbar} \delta_{\Gamma}(E_{\kappa_1\kappa_2\kappa_3\kappa_4}^{\text{HF}} - E_0^{\text{HF}}) \left| \langle \Phi_{\kappa_1\kappa_2\kappa_3\kappa_4}^{(i)} | \hat{V}_{\text{res}} | \Phi^{(i)} \rangle \right|^2 \quad (10b)$$

where δ_{Γ} is a δ function with finite width Γ . Detailed studies on the chosen numerical values of τ_{sample} and Γ are discussed in Secs. 3.2 and 3.3 respectively (see also [32, 17] for more details). $E_{\kappa_1\kappa_2\kappa_3\kappa_4}^{\text{HF}}$ and E_0^{HF} are the Hartree-Fock energies of the $2p2h$ and the original state respectively. It turns out that the sole matrix elements of the residual interaction which are non-vanishing for the STLM read :

$$\langle \Phi_{\kappa_1\bar{\kappa}_2\bar{\kappa}_3\kappa_4}^{(i)} | \hat{V}_{\text{res}} | \Phi^{(i)} \rangle = v_0 \sum_{\alpha, \alpha' > 0} A_{\alpha\kappa_1}^{(i)*} A_{\bar{\alpha}\bar{\kappa}_2}^{(i)*} A_{\bar{\alpha}'\bar{\kappa}_3}^{(i)} A_{\alpha'\kappa_4}^{(i)} \quad , \quad (11)$$

where all κ 's entering the latter equation are now positive. The decision to jump to $|\Phi_{\kappa_1\bar{\kappa}_2\bar{\kappa}_3\kappa_4}^{(i)}\rangle$ or to remain in the original state is done in Monte-Carlo fashion according to the probability $w_{\kappa_1\bar{\kappa}_2\bar{\kappa}_3\kappa_4}$. This is performed for each $|\Phi^{(i)}\rangle$ in the ensemble. The ensemble starts initially from the same state for all i . Then, each trajectory i develops its own dynamics through the stochastic choices described above. Finally, observables are computed for an ensemble average.

2.4. Exact propagation

The exact solution is conceptually the simplest but computationally most expensive. The fully correlated state is expanded into a complete basis of mean-field states

$$|\Psi\rangle = \sum_{\alpha_n, \alpha'_n > 0} c_{\alpha_1 \dots \alpha_{\Omega/2}, \bar{\alpha}'_1 \dots \bar{\alpha}'_{\Omega/2}} \hat{a}_{\alpha_1}^{\dagger} \dots \hat{a}_{\alpha_{\Omega/2}}^{\dagger} \hat{a}_{\bar{\alpha}'_1}^{\dagger} \dots \hat{a}_{\bar{\alpha}'_{\Omega/2}}^{\dagger} |\text{vac}\rangle . \quad (12)$$

The time-dependent Schrödinger equation

$$i\hbar\partial_t|\Psi\rangle = \hat{H}|\Psi\rangle \quad (13)$$

is solved by mapping it into a matrix equation for the expansion coefficients $c_{\alpha_1 \dots \alpha_{\Omega/2}, \bar{\alpha}'_1 \dots \bar{\alpha}'_{\Omega/2}}$. For the solution, we use again the Crank-Nicolson scheme (7), but now with the full Hamiltonian \hat{H} . The inverse $(1 + \frac{i dt}{2\hbar} \hat{H})^{-1}$ appearing therein is computed by solving a linear system using a bi-conjugate gradient stabilized method [33].

2.5. Initial excitation

As a first step, we have to prepare the ground state of the stationary problem. This is for TDHF and STDHF the Slater state with each $s_\alpha = -1$ s.p. state occupied and each $s_\alpha = +1$ unoccupied. For the exact solution, we have to solve the static Schrödinger equation with the full Hamiltonian \hat{H} .

The initial state for dynamical evolution is then obtained from the ground state by an instantaneous boost excitation

$$|\Phi(t=0)\rangle = e^{i\lambda(\hat{D} + \gamma\hat{W})} |\Phi_{\text{gs}}\rangle, \quad (14a)$$

$$\hat{D} = \sum_{m_\alpha} \left(\hat{a}_{1m_\alpha}^\dagger \hat{a}_{-1m_\alpha} + \hat{a}_{-1m_\alpha}^\dagger \hat{a}_{1m_\alpha} \right), \quad (14b)$$

$$\hat{W} = \frac{1}{2} \sum_{\alpha, \alpha' > 0} \left(\hat{a}_\alpha^\dagger \hat{a}_{\alpha'} + \hat{a}_{\alpha'}^\dagger \hat{a}_\alpha \right). \quad (14c)$$

The \hat{D} simulates a dipole operator of a typical many-particle system and the excitation operator $e^{i\lambda\hat{D}}$ induces initial $1p1h$ transitions within the same m_α . For example, one can consider the operator that couples a laser field to the electrons of an atom, and an instantaneous boost is the most generic excitation simulating a short pulse. The parameter λ tunes the strength of the initial excitation.

The \hat{W} operator serves a different purpose. At the mean-field level, the interaction (2c) deals only with vertical transitions which maintain the m quantum number. This emphasizes coherence which, in turn, overlays dissipation with large memory effects as we will see. To explore the level of dissipation in a more flexible manner, we stir up the interaction with transition across different m 's by applying the unitary transformation $e^{i\lambda\gamma\hat{W}} \hat{V} e^{-i\lambda\gamma\hat{W}}$ on the coupling \hat{V} with the mixing operator \hat{W} . This transformation maintains the overall interaction strength without rescaling v_0 . For simplicity, we apply the transformation to the initial state which turns out to be a good approximation to solving the dynamical equations with the modified interaction. The parameter γ quantifies the amount of mixing with respect to the dipole operator.

2.6. Observables

Our main aim here is to study the dynamics of thermalization after initial excitation. This is quantified by the fermionic entropy

$$S = -\text{Tr} [\hat{\rho} \ln \hat{\rho} + (1 - \hat{\rho}) \ln(1 - \hat{\rho})] . \quad (15)$$

where $\hat{\rho}$ is the one-body density operator whose matrix elements are the one-body density matrix $\rho_{\alpha'\alpha} = \langle \hat{a}_{\alpha'}^\dagger \hat{a}_{\alpha} \rangle$. A pure mean field state has $S = 0$. The entropy thus stays zero at all time in any TDHF calculation, while STDHF and the exact solution are expected to exhibit a time-dependent S .

A further test observable is the difference between one-body matrices in all combinations between TDHF, STDHF and the exact solution, quantified as

$$\delta_\rho = 2 \frac{\|\rho - \rho_{\text{ex}}\|}{\|\rho + \rho_{\text{ex}}\|} , \quad (16)$$

where $\|\dots\|$ stands for the Frobenius matrix norm $\|A\| = \sqrt{\text{Tr}(\hat{A}^\dagger \hat{A})}$.

2.7. Model parameters

We complete this section with specifying the values of the model parameters. To stay at the perturbative level for the correlations, the two-body interaction is taken relatively small, that is $v_0 = 0.05 \Delta$. We propagate TDHF and the exact solution using the Crank-Nicolson scheme with a time step $dt = 0.01 \Delta^{-1}$.

The number of particles varies from $\Omega = 4$ to 10 in the comparison between the exact solution and the STDHF. Due to an exponentially increasing computing time for the exact propagation, the cases from $\Omega = 12$ to 20 have been explored in the STDHF scheme only. The number of samples in the STDHF ensemble is always $\mathcal{N}_{\text{ens}} = 100$. We have checked also larger ensembles and found practically the same results.

We have tested various values of the mixing parameter γ , from 0 to 0.6. In the following results, it is set to 0.3 since such a value creates enough disorder at $t = 0$, that is the needed transitions for STDHF to operate (see discussion in Sec. 2.5). Figure 2 shows the excitation energy E^* attained as a function of λ in the case of 10 particles, a band width $\sigma = 0.2 \Delta$ and an interaction strength $v_0 = 0.05 \Delta$. The energy grows monotonously up to a maximum where it turns to monotonous decrease. The upper limit of E^* reflects the fact that the model Hamiltonian is bound not only from below,

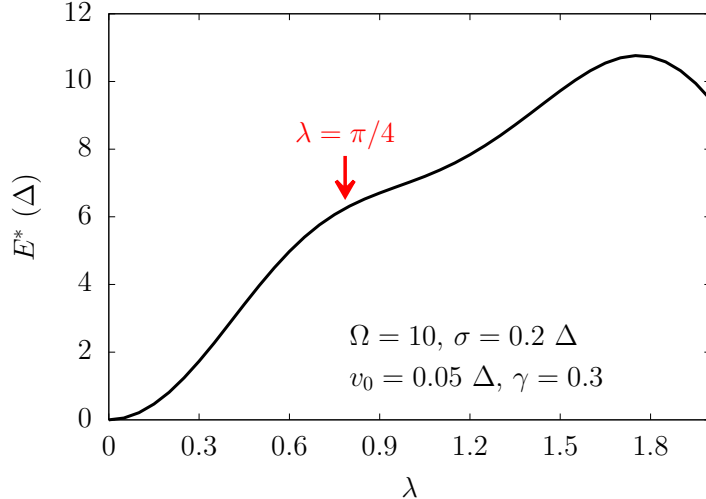


Figure 2: Accessible excitation energy E^* (in Δ units) as a function of λ for the initial excitation (14) with $\gamma = 0.3$, and the other STLTM parameters as indicated.

as it should be for a non-relativistic Hamiltonian, but also from above. The relevant range of the STLTM stays in the region of λ safely below the turning point (which is at $\lambda = \pi/2$ for $\gamma = 0$). In practice, we use $0.6 \leq \lambda \leq 0.8$ close to $\pi/4$ which corresponds to a state with the particles having half weight in the upper band and half weight in the lower band. This value for λ is safely in the regime of increasing E^* . We have checked that the cases $\gamma = 0$ and $\gamma = 0.3$ provide moderate differences in E^* . This corroborates the above statement that the overall interaction strength is little affected by virtue of scanning interactions in terms of a unitary transformation.

3. Results

3.1. A first test case

We start with the analysis of a typical test case from the perspective of the difference of s.p. density matrices, the entropy, and the expectation value of the dipole. The time evolution of these observables is displayed in Fig. 3. In the upper panel, we compare the density matrix ρ obtained in HF and that in STDHF with respect to the exact density matrix ρ_{ex} in terms of norm of the difference δ_ρ , defined in Eq. (16), of TDHF or STDHF with respect to the exact solution. STDHF provides a much smaller deviation δ_ρ than TDHF.

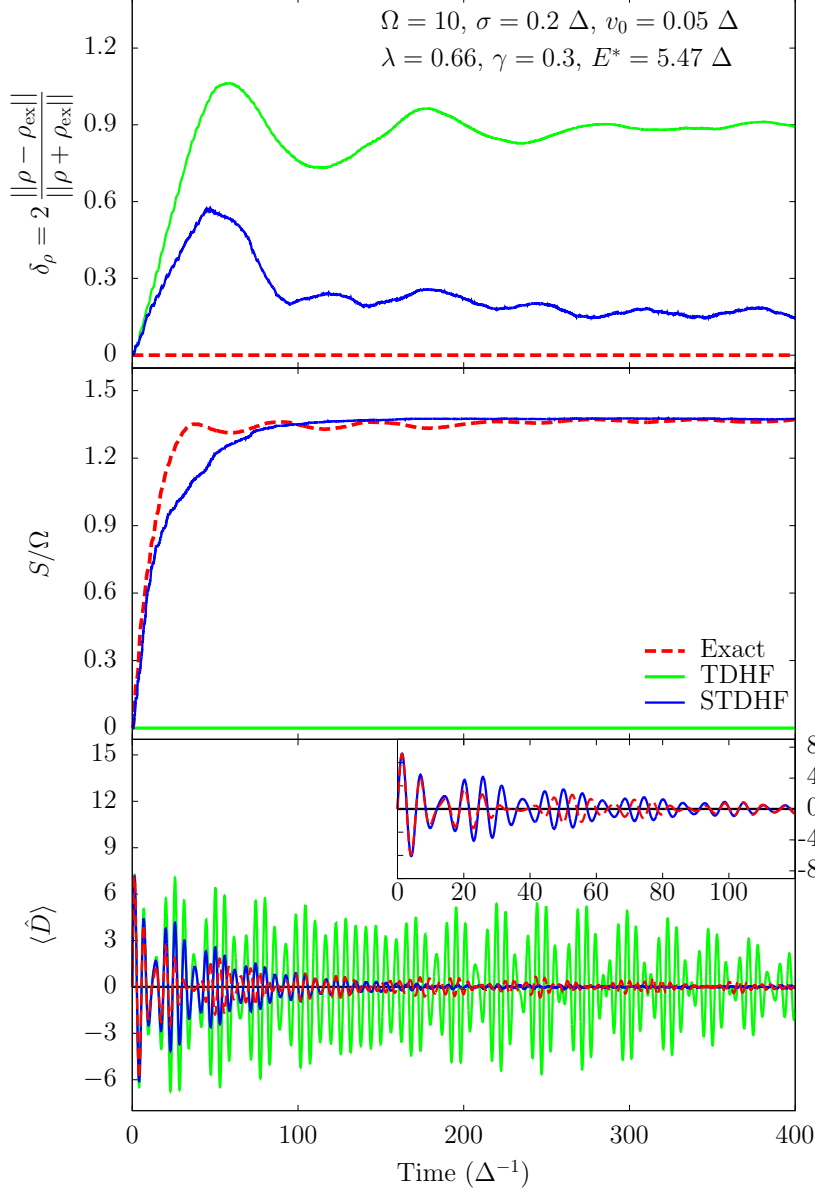


Figure 3: Comparison of TDHF, STDHF and exact solution with respect to three observables, as a function of time, with the STLM parameters as indicated. Bottom : expectation value of the dipole operator \hat{D} , see Eq. (14b), with as an insert a zoom on the exact and the STDHF responses below $120 \Delta^{-1}$. Middle : entropy per particle S/Ω , see Eq. (15). Top : difference of one-body density.

This indicates that STDHF is indeed able to incorporate a great deal of the dynamical correlations. Both deviations are composed from a global trend plus oscillations. The trend approaches a rather large stable deviation δ_ρ for TDHF and seems to indicate (slow) convergence to negligible deviation for STDHF.

These oscillations are also observed in the time evolution of the exact entropy per particle, see middle panel of Fig. 3. The entropy from STDHF reproduces the exact entropy in the average trend and in the asymptotic value rather well, see also Figure 7 and the related discussion. The main discrepancies lie in the lack of oscillations. Indeed, the instantaneous (Markovian) approximation when evaluating the stochastic jumps in STDHF erases at once all coherence and memory effects. Similar features are seen in semi-classical VUU models where the collision term is also treated in Markovian approximation. The oscillating entropy for the exact solution shows that the STLM still carries a substantial amount of memory effects which can only be coped with using a frequency (or time) dependent kernel for the jump probability [34]. The TDHF result (light green line) differs dramatically from STDHF. It maintains zero entropy throughout and never relaxes to anything like a thermalized state. It cannot reproduce at all the long-time behavior of system as soon as dissipation becomes relevant.

It is also interesting to note that the maximum value of entropy $S/N = 2 \log 2 \simeq 1.38$ corresponds to an equidistribution of $N = 10$ particles over all $2\Omega = 20$ states with occupation probability $w_\alpha = \rho_{\alpha\alpha} = 1/2$. To that extent, the agreement at the maximum is sort of trivial. However, the STDHF results follow the exact curve also down to lower values and agree as long as the STDHF jumps have their grip. This is the non-trivial result indicating that STDHF catches the basic statistical properties of the system.

The lower panel of Fig. 3 shows the evolution of dipole momentum for the three solution schemes. This confirms what we had seen already from the two other observables. TDHF shows long standing oscillations and reverberations and thus stays far off the exact solution. STDHF, on the other hand, constitutes a remarkable improvement, in particular over the first $120 \Delta^{-1}$. STDHF is thus providing a reliable description of dissipation. A slight difference comes up at later times. The exact solution shows some reverberations which are absent in STDHF. These reverberations are related to the oscillations in entropy and thus an effect of quantum coherence deliberately suppressed in STDHF. But this is a small effect and the generally good agreement prevails.

This first example shows strengths and weaknesses of STDHF. It is a therefore a great improvement as compared to TDHF in that it properly catches the dissipative aspects of many-dynamics and produces in due time the correct asymptotic state (thermal equilibrium). However, STDHF implies a Markovian approximation (that is, instantaneous jumps) and is unable to incorporate memory effects. It then depends on the system and dynamical regime how important memory effects are.

The three observables shown in Fig. 3 are of different nature and show different aspects of the system. Dipole momentum $\langle \hat{D} \rangle$ and one-body entropy S are both one-body observables where S characterizes the state of the system while $\langle \hat{D} \rangle$ demonstrates measurable consequences of dissipation. The information concerning dissipation is comparable. We prefer in the following the entropy S because it displays the simpler signal.

The norm of the difference of full density matrices, δ_ρ , is a many-body observable and so also carries many-body information not accounted for in comparing one-body entropies. Still, δ_ρ and S deliver comparable information to the extent that STDHF is much closer to the exact solution than TDHF. There is a faint difference too: δ_ρ is more critical as it shows always a small, but finite, value for STDHF, indicating the known fact that STDHF unavoidably sacrifices parts of the exact solution, namely the coherent correlations. We are interested here in an appropriate reproduction of dissipation which is biased in incoherent correlations. The one-body entropy S is the more appropriate measure for this purpose. We thus confine the further examples to the entropy only.

3.2. Impact of the sampling time

Two important ingredients of the STDHF transition probability given in Eq. (10b) are the sampling time τ_{sample} and the finite width of the δ_Γ function, see [17] for a detailed discussion. We here specifically explore the impact of the first one in the studied model. Indeed, τ_{sample} has to be large enough such that the oscillations of the wave functions' phase satisfy the δ_Γ function. On the other hand, it should be small enough to resolve the temporal changes of the mean-field. In addition, it should remain smaller than the total jump rate, i.e.

$$\tau_{\text{sample}} \leq \left(\sum_{\kappa_1, \kappa_2, \kappa_3, \kappa_4} \mathcal{P}_{\kappa_1 \kappa_2 \kappa_3 \kappa_4} \right)^{-1} . \quad (17)$$

Figure 4 illustrates the impact of the variation of τ_{sample} on the example of the detailed time evolution of the one-body entropy. τ_{sample} ranges from

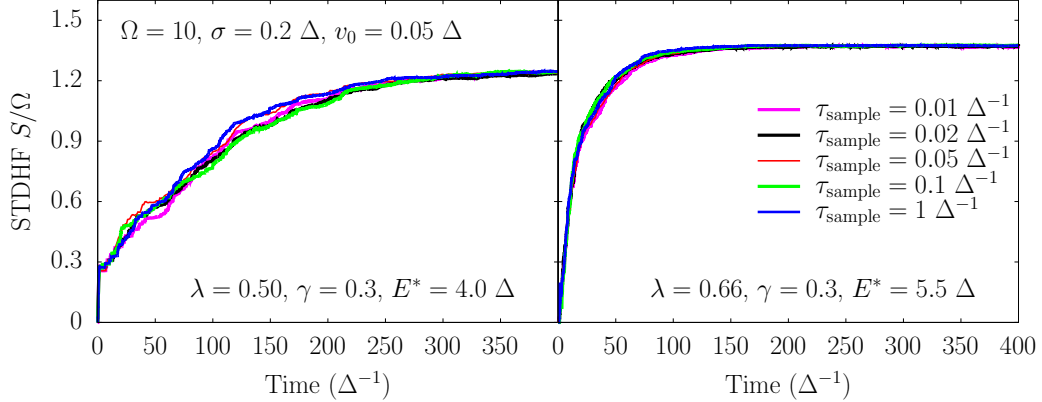


Figure 4: Time evolution of one-body entropy S for 5 different sampling times τ_{sample} as indicated, and for two different excitation energies, $E^* = 4.0 \Delta$ (left) and 5.5Δ (right).

$0.01 \Delta^{-1}$ to $1 \Delta^{-1}$, that is over two orders of magnitude. The corresponding results are stable within this rather broad parameter window. Note however that, for some values of E^* , the case $\tau_{\text{sample}} = 0.1$ or $1 \Delta^{-1}$ exceeds the total transition rate. Therefore, in all the following results, we have set $\tau_{\text{sample}} = 5 dt = 0.05 \Delta^{-1}$ to stay on the safe side and to satisfy inequality (17).

3.3. Impact of the finite width Γ

We now discuss the influence of the finite width Γ of the δ function entering Eq. (10b). Unlike semi-classical cases where we deal with a continuum [9, 31], such a finite width is necessary in a discrete quantum spectrum to grab all possibly relevant transitions. However, it should be chosen small enough to maintain an acceptable energy conservation [32, 17]. In practice, the δ_Γ function is approximated by a fixed window

$$\delta_\Gamma(x) = \begin{cases} 1/\Gamma & \text{for } |x| < \Gamma/2 \\ 0 & \text{for } |x| \geq \Gamma/2 \end{cases} . \quad (18)$$

Figure 5 demonstrates the effect of Γ which has been varied from $10^{-4} \Delta$ to 0.1Δ . The smallest values $\Gamma = 10^{-4} \Delta$ and $5 \times 10^{-4} \Delta$ are obviously too low and do not produce enough jumps to provide the right rise of the one-body entropy S at short times, see upper panel. All higher values yield

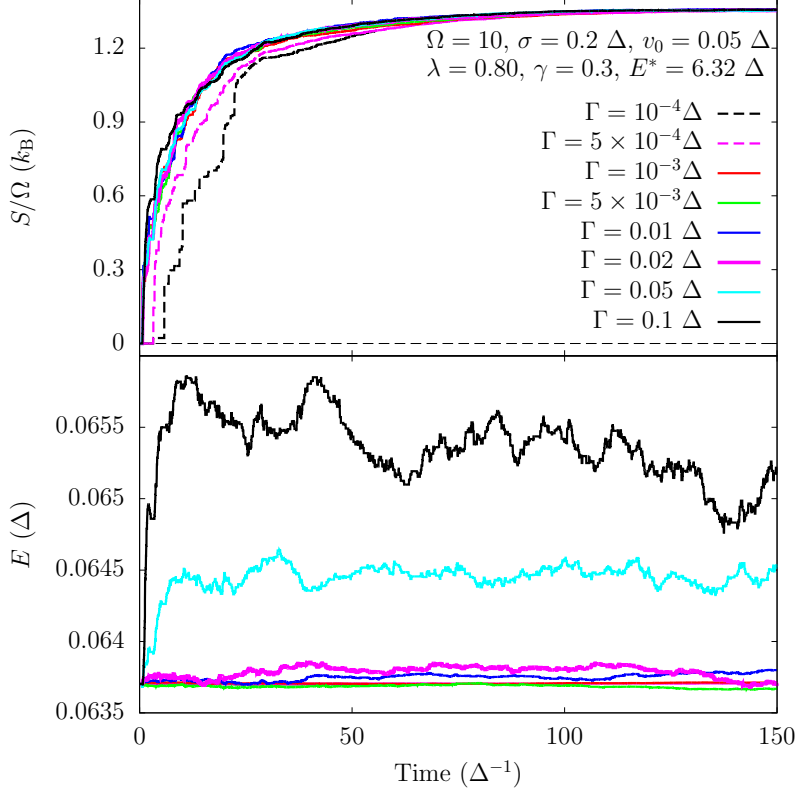


Figure 5: Time evolution of one-body entropy S (upper panel) and total energy (lower panel) for different values of the energy width Γ in the energy criterion δ_Γ of the STDHF jump probability, see Eq. (10b).

the same pattern for S and thus reproduce correctly the dissipation from two-body transitions. On the other hand, as expected, energy conservation (lower panel) is degraded with increasing Γ . Note however the narrow scale for energy in the plot. Even the worst case still shows a fair energy conservation. The values of Γ up to $2 \times 10^{-2} \Delta$ deliver a good compromise between appropriate dissipation and energy conservation. Our chosen value in the following analysis is $\Gamma = 0.02 \Delta$ and constitutes the best compromise in this respect.

We have also checked the effect of the actual profile of the δ_Γ function by comparison with a Gaussian instead of the box distribution (18). The differences are marginal. We have therefore preferred the box distribution

because it is by definition limited and does not have the danger of occasional outliers as infinite distributions like Gaussians have.

3.4. Varying the excitation energy

Dissipation is usually weak in the regime of low excitations and acquires importance only for sufficiently large excitation energy [7]. Stochastic evaluation of dynamical correlations as done in STDHF or VUU is designed for high excitation energies where the phase space for jumps is (hopefully) dense enough. It is thus of interest to check the performance with varying excitation energy $E^* = E - E_{\text{g.s.}}$ which is the difference between the actual (conserved) energy E of the system and the ground-state energy $E_{\text{g.s.}} = -\sum_{m_\alpha} \varepsilon_{-1, m_\alpha}$.

Figure 6 shows the asymptotic one-body entropy S_{lim} as a function of E^* (in the branch of increasing excitation energy, see discussion of Fig. 2). The

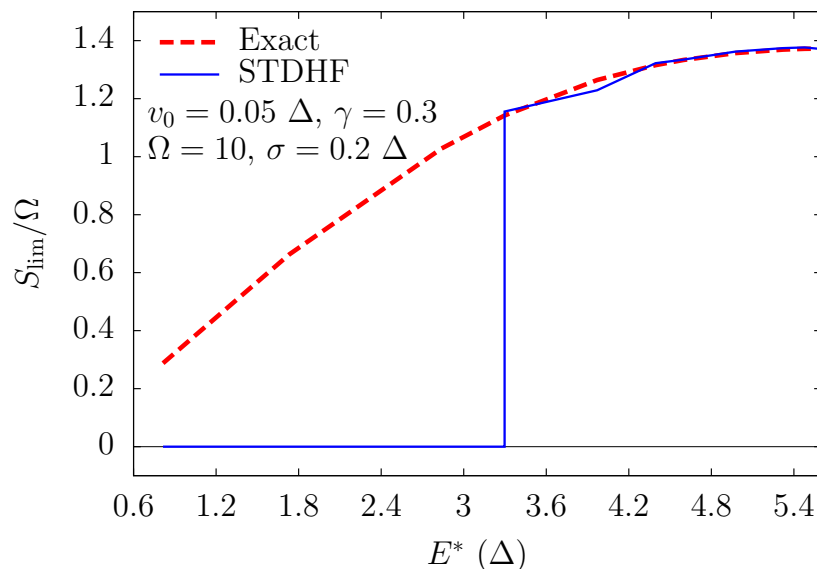


Figure 6: Asymptotic entropy per particle S_{lim}/Ω for the exact solution (thick curves) and for STDHF (thin curves), as a function of the excitation energy E^* obtained by scan of initialization strength λ , see Eq. (14), and the other parameters of the model as indicated.

exact solution shows a smooth and monotonous increase. STDHF behaves much different in that it shows a threshold behavior. It remains inactive for $E^* < 3.3 \Delta$ and suddenly switches to reproduce the exact value once

the stochastic jumps get their grip. The result confirms that STDHF is an approach for sufficiently high excitation energy. We have also explored a profile different from a box function for the finite δ_Γ function defined in Eq. (18), namely we have tested a Gaussian instead. The energy threshold slightly depends on the profile chosen for δ_Γ but the asymptotic value S_{lim} remains unchanged regardless δ_Γ or even the width Γ itself.

A comment about maximum value of the entropy shown in Fig. 6 is in order. It comes very close to the value $S/\Omega = 2 \log 2 \approx 1.38$. As already discussed in Sec. 3.1, it stands for equi-partition $\rho_{\alpha\alpha} = N/(2\Omega) = 1/2$ and is the maximally possible value for S/Ω . The figure shows that, in the given mode, STDHF comes to work only for rather flat distributions of $\rho_{\alpha\alpha}$ with significant occupation of the upper band, thus having S/Ω near the maximum.

3.5. Impact of band width

Next, we explore the effect of band width σ by varying it in four steps : $\sigma = 0.05, 0.2, 0.5$ and 0.8Δ . The other model parameters are kept fixed at $\Omega = 10$, $\lambda = 0.8$ and $\gamma = 0.3$. Figure 7 compares the time evolution of the entropy between exact solution and STDHF. Decreasing σ reduces the oscillations of the exact entropy and yields generally faster relaxation to equilibrium (= maximum entropy). This is plausible because smaller σ produce larger density of states which, in turn, enhances the chances for jumps and thus delivers more dissipation. A larger σ spreads the spectrum instead and dramatically reduces the phase space accessible to jumps. Only few states remain in communication and with it, only few frequencies compete which, in turn, leave longer reverberation before reaching equilibrium.

STDHF, as expected, is unable to follow the oscillations. But it nicely reproduces the trend to increasing relaxation times with increasing σ . Indeed, for the same reasons as before, increasing σ decreases the probability of $2p2h$ transitions and therefore, provides a slower relaxation time of the STDHF entropy as well. The average predictions are thus still reliable.

3.6. Varying the number of particles

Variation of σ as done in the previous section changes the density of states together with energy span for the jumps. We complement that by varying the particle number Ω . Here, we keep the ratio σ/Ω constant (at the value of 0.02). In such a way, the density of states is kept constant. Increasing Ω at constant σ would amount to increase the density of states (as one does when

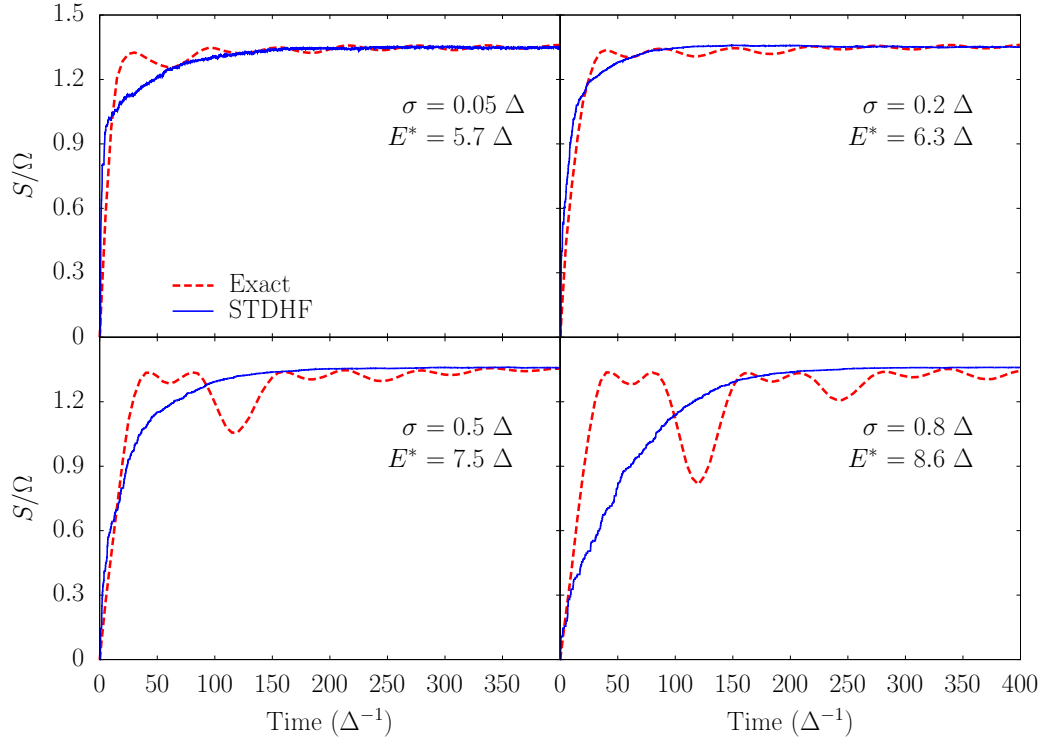


Figure 7: Entropy per particle S/Ω as a function of time as obtained from exact solution (dashed lines) and STDHF (full lines). The four panels show results for four different values of band width σ as indicated. The other parameters are : $\lambda = 0.8$, $\gamma = 0.3$, $\Omega = 10$ and $v_0 = 0.05 \Delta$. The corresponding excitation energy E^* depends on σ and is also indicated in the plots.

increasing σ at constant Ω). Since the corresponding results (not shown) are very similar to those presented below, we here focus on the impact of increasing the number of particles at constant density of states.

Figure 8 shows the time evolution of the entropy for the exact solution (left panel) and for STDHF (right panel). We start at $\Omega = 6$ because STDHF

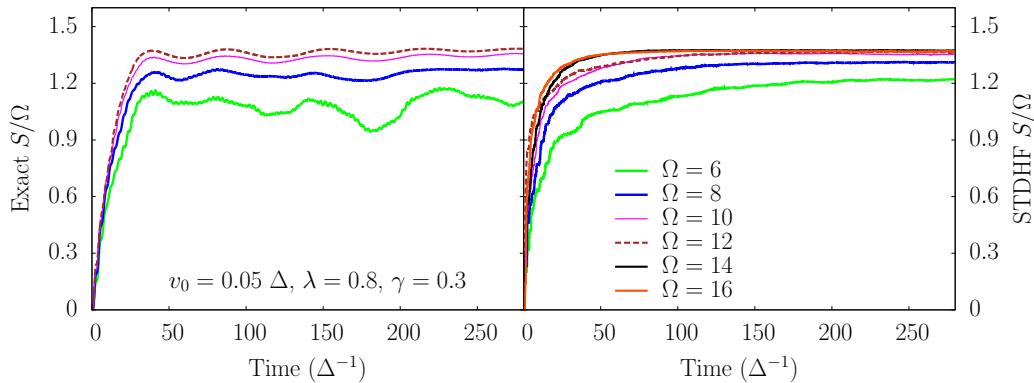


Figure 8: Time evolution of the entropy per particle S/Ω for exact solution (left) and STDHF (right) and for different numbers of particles Ω as indicated, while keeping the ratio $\sigma/\Omega = 0.02$. The other model parameters were : $v_0 = 0.05 \Delta$, $\lambda = 0.8$, $\gamma = 0.3$.

does not become active for smaller Ω . At the upper end, we go up to $\Omega = 12$ for the exact calculation and checked two higher values of Ω for STDHF. As we could expect from the previous results, the amplitude of oscillations of the exact entropy indeed shrinks with increasing Ω since the number of states also increases. We also see a faster relaxation for increasing Ω , again related to increasing number of states. This trend to decreasing relaxation time with increasing Ω is also reproduced by STDHF. We therefore expect that the larger the Ω , the better the agreement between the exact and the STDHF dynamics. We also observe a convergence of the STDHF results at $\Omega = 14$ since the time evolution of the entropy changes very little when going from $\Omega = 14$ to $\Omega = 16$.

There is a further interesting feature. The entropy indicates two phases of relaxation. It starts with a fast relaxation at early times and bends over to a different rate at around $20\text{--}30 \Delta^{-1}$. This property is probably also present in the exact solution although masked by the oscillations.

4. Conclusion and perspectives

We have investigated the Stochastic Time-Dependent Hartree-Fock (STDHF) approach in a schematic model which allows a comparison with the exact solution. The model consists of N fermions in two bands of single-particle (s.p.) levels, the lower one fully occupied and the upper one empty. This is augmented by a two-body interaction, which is motivated first from a typical pairing interaction and modified by gradually mixing more and more couplings between different s.p. levels. The model has much in common with quasi-spin models consisting out of N coupled spin 1/2 systems, which are widely used in many areas of physics. The actual tests here are run in the regime of small interaction strength to maintain a clear hierarchy of s.p. motion and two-body collisions. For the ground state, we thus see little difference between Hartree-Fock and exact solution because static correlations are weak. The other model parameters are the number of particles, the band gap, the band width, and the mixing of transitions in the two-body interaction. The band gap is taken as the unit of energy and all other energies count relative to it. The number of particles divided by the band gap yields the density of states which is a crucial parameter determining the amount of dissipation by dynamical correlations. The dynamical evolution is initialized through an instantaneous boost by a "dipole" operator, which in the schematic model is a one-body operator collecting coherently all vertical transitions between the two bands. The strength of boost determines the excitation energy which is one further crucial parameter for the amount of dissipation.

Although the model is built to be very simple, the exact solution limits the affordable system size. Actually we could perform tests up to 12 particles. On the other hand, a dissipative model as STDHF relies on a high density of states to achieve a good mixing of frequencies and so to justify the Markovian approximation implied in the concept of instantaneous jumps between two-particle configurations. The limited particle number means that we are exploring STDHF in a critical regime and that the situation may be more forgiving in large systems. Even for this limited system size, we find that STDHF provides a substantial improvement as compared to mere time-dependent Hartree-Fock (TDHF): STDHF drives convergence to the same final one-body state as the exact solution and the relaxation rate is of the correct order. A major difference remains concerning memory effects. STDHF ignores by construction (Markovian approximation) memory effects.

The exact solution, however, shows such memory effects which, e.g., lead to oscillations of the one-body entropy. Varying the model parameters allowed to explore the dependence of memory effects on dynamical regime and system properties. Memory effects fade away with increasing excitation energy, and increasing density of states. In situations where memory effects are small, we find a good agreement of STDHF with the exact solution. If some oscillations remain in the time evolution of the entropy, we see at least that STDHF is still providing a reliable picture of the general trend and of the final state. Thus the result is very encouraging on the one hand, but also sets a warning flag which reminds us to check Markovian approximation in each new situation. The case of non half-filled systems also opens the road for new aspects, especially at the side of the time evolution of the one-body entropy. Work in that direction is in progress.

Acknowledgments

This work was supported by the CNRS and the Midi-Pyrénées region (doctoral allocation number 13050239), and the Institut Universitaire de France. It was granted access to the HPC resources of IDRIS under the allocation 2014–095115 made by GENCI (Grand Equipement National de Calcul Intensif), and of CalMiP (Calcul en Midi-Pyrénées) under the allocation P1238.

References

- [1] E. K. U. Gross, J. F. Dobson, M. Petersilka, *Top. Curr. Chem.* **181** (1996) 81.
- [2] M. A. L. Marques, E. K. U. Gross, *Ann. Rev. Phys. Chem.* **55** (2004) 427.
- [3] T. Fennel, , K.-H. Meiwes-Broer, J. Tiggesbäumker, P.-G. Reinhard, P. M. Dinh, E. Suraud, *Rev. Mod. Phys.* **82** (2010) 1793.
- [4] K. T. R. Davies, K. R. S. Devi, S. E. Koonin, M. R. Strayer, in: D. A. Bromley (Ed.), *Treatise on Heavy-Ion Physics*, Vol. 3 *Compound System Phenomena*, Plenum Press, New York, 1985, p. 3.
- [5] C. Simenel, *Eur. Phys. J. A* **48** (2012) 152.

- [6] J. A. Maruhn, P.-G. Reinhard, P. D. Stevenson, A. S. Umar, *Comp. Phys. Comm.* **185** (2014) 2195.
- [7] L. P. Kadanoff, G. Baym, *Quantum Statistical Mechanics*, Benjamin, New York, 1962.
- [8] R. Balescu, *Equilibrium and non equilibrium statistical mechanics*, Wiley, New York, 1975.
- [9] G. F. Bertsch, S. Das Gupta, *Phys. Rep.* 160 (1988) 190.
- [10] D. Durand, E. Suraud, B. Tamain, *Nuclear Dynamics in the Nucleonic Regime*, Institute of Physics, London, 2000.
- [11] A. Doms, P.-G. Reinhard, E. Suraud, *Phys. Rev. Lett.* 81 (1998) 5524.
- [12] T. Fennel, G. F. Bertsch, K.-H. Meiwes-Broer, *Eur. Phys. J. D* 29 (2004) 367.
- [13] A. Nitzan, M. A. Ratner, *Science* 300 (2003) 1384.
- [14] P.-G. Reinhard, E. Suraud, *Ann. Phys.* 216 (1) (1992) 98–121.
- [15] D. Lacroix and S. Ayik, *Eur. Phys. J. A* 50 (6) (2014) 95.
- [16] E. Suraud, P.-G. Reinhard, *New J. Phys.* 16 (2014) 063066.
- [17] N. Slama, P.-G. Reinhard, E. Suraud, *Ann. Phys. (N.Y.)* 355 (2015) 182.
- [18] H. J. Lipkin, N. Meshkov, A. J. Glick, *Nucl. Phys.* 62 (2) (1965) 188–198.
- [19] N. Meshkov, A. J. Glick, H. J. Lipkin, *Nucl. Phys.* 62 (2) (1965) 199–210.
- [20] A. J. Glick, H. J. Lipkin, N. Meshkov, *Nucl. Phys.* 62 (2) (1965) 211–224.
- [21] G. Holzwarth, *Nucl. Phys. A* 207 (1973) 545–564.
- [22] G. Jaeger, *Quantum information: an overview*, Springer, Berlin, 2006.
- [23] A. P. Severyukhin, M. Bender, P.-H. Heenen, *Phys. Rev. C* 74 (2006) 024311.
- [24] D. Lacroix, S. Ayik, B. Yilmaz, *Phys. Rev. C* 85 (2012) 041602(R).

- [25] B. Yilmaz, D. Lacroix, R. Curebal, *Phys. Rev. C* 90 (2014) 054617.
- [26] D. Lacroix, Y. Tanimura, S. Ayik, B. Yilmaz, *Eur. Phys. J. A* 52 (2016) 94.
- [27] P.-G. Reinhard, A. S. Umar, K. T. R. Davies, M. R. Strayer, S.-J. Lee, *Phys. Rev. C* 37 (3) (1988) 1026–1035.
- [28] P. Ring, P. Schuck, *The Nuclear Many-Body Problem*, Springer–Verlag, New York, Heidelberg, Berlin, 1980.
- [29] J. Maruhn, P.-G. Reinhard, E. Suraud, *Simple models of many-fermions systems*, Springer, Berlin, 2010.
- [30] J. Crank, P. Nicolson, *Mathematical Proceedings of the Cambridge Philosophical Society* 43 (01) (1947) 50–67.
- [31] Y. Abe, S. Ayik, P.-G. Reinhard, E. Suraud, *Phys. Rep. C* 275 (1996) 49.
- [32] L. van Hove, *Physica* 21 (1955) 517.
- [33] H. A. van der Vorst, *SIAM J. Sci. and Stat. Comput.* 13 (2) (1992) 631–644.
- [34] C. Greiner, K. Wagner, P.-G. Reinhard, *Phys. Rev. C* 49 (1994) 1693.